Charmed particles production in pA-interactions at 70 GeV

Vasily Ryadovikov[1],[⋆]
(on behalf of the SVD Collaboration)

[1]*Institute for High Energy Physics, Sq. Nauki 1, Protvino, Moscow region 142281, Russia*

Abstract. The results of the SERP-E-184 experiment at the U-70 accelerator (IHEP, Protvino) are presented. Interactions of the 70 GeV proton beam with carbon, silicon and lead targets were studied to detect decays of charmed D^0, $\bar{D}^0$, D^+, D^- mesons and Λ_c^+ baryon near their production threshold. Measurements of lifetimes and masses have shown a good agreement with PDG data. The inclusive cross sections of charm production and their A-dependencies have been obtained. The yields of these particles are compared with the theoretical predictions and the data of other experiments. The measured cross section of the total open charm production $\sigma(c\bar{c}) = 7.1 \pm 2.3(stat) \pm 1.4(syst)$ μb/nucleon at the collision c.m. energy $\sqrt{s} = 11.8$ GeV is well above the QCD model predictions. The contributions of different kinds of charmed particles to the total cross section of the open charm production in proton-nucleus interactions vary with energy.

1 Introduction

We represent the results of data processing of E-184 experiment on studying of charmed particles production mechanisms in pA-interactions at 70 GeV. The experiment is carried out by Cooperation SINP MSU (Moscow) – JINR (Dubna) – IHEP (Protvino) at the U-70 accelerator in Protvino. Importance of work is that:
- The majority of experiments on a charm are executed with the electron beams where their main properties are studied (measurements of mass, decay branching etc.).
- The experiments with hadron and heavy ion beams gave an opportunity to study the mechanisms of charmed particle production in varying nuclear media from threshold energies to energies of LHC.
- The charm production by hadrons is sensitive to the medium modifications. The charmed particles are good probes to investigate properties of this medium, which may show up as quark-gluon plasma.
- More then 20 years ago in IHEP the measurements of cross sections of the charmed particle production at the near-threshold energy region were performed by beam-dump experiment with an absorber of muons [1], by the SCAT bubble chamber experiment [2] and by the experiment with BIS-2 spectrometer [3]. The measured total cross sections in the energy range of the primary beam from 40 to 70 GeV have proved to be much higher than the model predictions based on QCD.
Experiment of E-184 is carried out on the Spectrometer with Vertex Detector setup (SVD).


[⋆]e-mail: riadovikov@ihep.ru

2 SVD setup detectors

The main elements of the setup for charm searching [4] are the high-precision micro-strip vertex detector (MSVD) with an active target (AT) and a magnetic spectrometer (MS) of the aperture equal to 1.8 x 1.2 m2 and the field of 1.18 T within the region 3 m long. The active target (AT) (Fig. 1) contains 5 Si-detectors each 300 μm thick and 1-mm pitch strips, the Pb-plate (220 μm thick) and C-plate (500 μm thick). The micro-strip tracking part of MSVD consists of 10 Si-detectors.
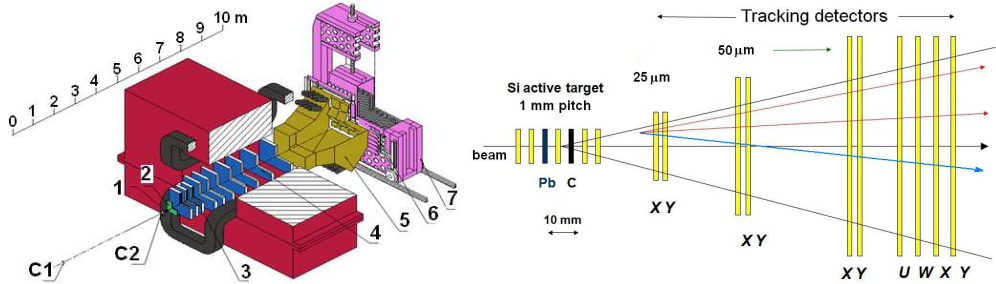
Figure 1. SVD-2 layout and scheme of MSVD. C1,C2 - beam scintillation counters; 1 - Si active target (AT); 2 - microstrip vertex Si-detector (MSVD); 3, 4 - MWPC of magnetic spectrometer (MS); 5 - threshold Cherenkov counter (CC); 6 - scintillation hodoscope (SC); 7 - detector of gamma-quanta (DEGA).
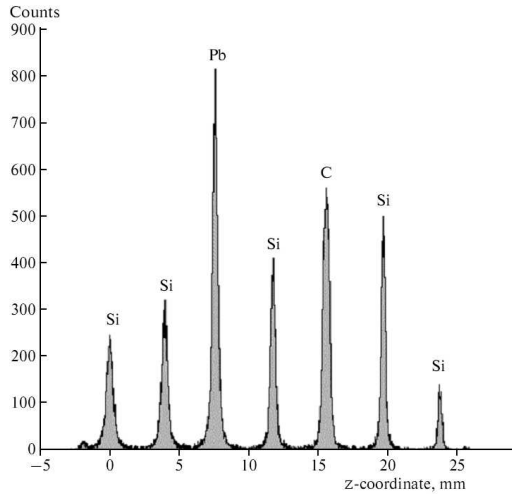
Figure 2. The reconstructed Z-coordinates of the primary vertices in AT.

The vertex detector plays the main role in search of secondary vertexes with possible decays of a charm as the distance between a point of interaction and D meson decay point doesn't exceed 2 mm. We have the accuracy of primary vertex reconstruction along a beam of 100 microns (Fig. 2), secondary vertex – 200 microns. The coordinate accuracy is equal to 10 microns in the cross plane. The spectrometer features allow one to get the effective mass resolution of σ = 4.4 MeV/c^2 for K_s^0 and 1.6 MeV/c^2 for Λ^0 masses, for the particles decayed before the MSVD tracking detectors.

3 Simulations and data processing

Modeling is needed for:
- to optimize of event selection criteria. As a result of modeling selection criteria of events with the minimum background were taken;
- to define the detection efficiency for a charm particle;
- to confidence that we have really charm particles by the comparison of parameters (decay length, etc.) of MC and experimental data of charm particles decays.

Proton-nucleus interactions have been simulated by means of FRITIOF7.02 code [5]. The Fermi motion of nucleons, the deformation of nucleus and multiple re-scattering are taken into account. The nucleon distribution density in a nucleus is described in our case by the Woods–Saxon potential $\rho(r) = \rho(0)/(1 + exp[(r - r(0) \cdot A^{1/3}]/c)$, with $r(0) = 1.16(1 - 1.16A^{-2/3})$ fm and c = 0.5 fm. Hadronization processes described by the Lund scheme using the fragmentation function $f(z) \sim z^{-1}(1 - z)^\alpha \cdot exp(-bm_t^2/z)$. The parameters of this function were chosen as a = 0.18 and b = 0.34 GeV^{-2} in accordance with the results of the e^+e^- experiments OPAL [6] and [7] where the parameters were adjusted by the measured spectra of D and D^* mesons. Default values were used for the remaining parameters in the FRITIOF code.

GEANT3.21 package [8] was used to simulate registration of pA-interactions. The geometry of active and passive elements of the setup have been defined by means of metrological measurements and corrected with results of the "straight tracks" software alignment. The measured grid map of the magnetic field was applied. Charge spreading over the MSVD strips, noises and cutoff amplitudes were introduced channel-by-channel in accordance with experimentally measured values and data acquisition parameters. The actual efficiencies obtained experimentally for the proportional wire chambers were used for the magnetic spectrometer.

The simulated events have been processed by really using data handling system of the SERP-E-184 experiment. The common data processing procedure started with the filtration of MSVD data and reconstruction of tracks and primary vertices [9]. Next, we selected events with the secondary vertices close to the interaction points as the candidates for charm-production events. For this purpose the method of an analysis in the space of track parameters [10] was used. In this space each track is presented with a point and all points for the tracks from the same vertex are located on a straight line. The results of simulation were compared with the experimental data. A good agreement was found for the numbers of minimum bias events in each of AT plates, for multiplicities of charged particles in primary vertices and for their momenta.

In case of $D^0(\bar{D}^0) \to K\pi$ process the detection of $K_s^0 \to \pi\pi$ decay in the MSVD can serve as a reference procedure, because the well-known kaon production cross section is many times larger than for charmed particles. It has been used to estimate the detection efficiency of V^0 decay near the primary vertex and validate the data processing algorithms for $D^0(\bar{D}^0)$ [11].

Additionally, the background minimum bias events were simulated without charm production. This procedure was necessary to estimate the background conditions. The characteristics of three-prong systems ($K\pi\pi$ and $pK\pi$) for MC events were compared to the experimental data [12], [13]. There is a good agreement between the simulated and experimental distributions for a path length, momentum and x_F variable ($x_F = p_L/\sqrt{s}$ in c.m.s.).

4 Selection of events with charmed particles

We have 52 million inelastic events in AT (C, Si, Pb).

4.1 $D^0 \rightarrow K^-\pi^+$, $\bar{D}^0 \rightarrow K^+\pi^-$ decays

The candidates for the events with D^0 or $\bar{D}^0$ particle and its decay into $K\pi$ system were selected using the following criteria [11]:

(i) The distance between the primary vertex and the V^0 vertex is more than 0.5 mm.

(ii) The decay tracks of the V^0 particle have non-zero impact parameters with respect to the primary vertex, and the track of V^0 particle points to the primary vertex.

(iii) The effective mass of the $K\pi$ system differs from the world-average value of the D^0 mass (1.865 GeV/c^2) by less than 0.5 GeV/c^2.

(iv) The momentum of the $K\pi$ system is higher than 10 GeV/c.

(v) The transverse momentum of the decay particle with respect to the direction of motion of the $K\pi$ system is higher than 0.3 GeV/c. It follows from the analysis of the Armenteros–Podolansky criterion and suppresses the background from neutral kaons and Λ^0 hyperons decays (Fig. 3 left).

(vi) Having a rather small number of events, the candidates for the $(D^0/\bar{D}^0)$ particles were visually inspected by means of a specially designed graphic package on an high resolution PC screen. In this way, hits which were not included into the reconstructed tracks in MSVD are tested. Using those hits and the visual picture of the event helps to eliminate obviously the background events with beam tracks, secondary interactions at AT, pile-up and ghost tracks.
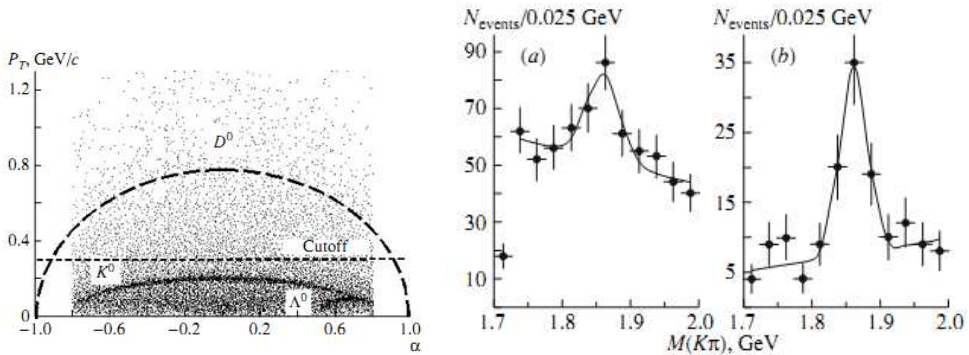
Figure 3. Left: Armenteros–Podolansky plot for K^0, Λ^0 and D^0; $\alpha = (P_L^+ - P_L^-)/(P_L^+ + P_L^-)$. Right: Effective mass spectra of the $K\pi$ system (a) before and (b) after visual inspection.

The effective mass spectra of the $K\pi$ system after applying the criteria (i-v) and visual inspection of the events are presented in Figs. 3a and 3b (right). The mass interval for the visual inspection has been limited to the region from 1.7 to 2.0 GeV/c^2. The visual inspection significantly reduces the background in the region of interest, but the charm + anti-charm $(D^0/\bar{D}^0)$ signal decreased only on 20%. The data fit by the sum of the straight line and the Gaussian function is shown in Fig. 3b (right). It gives 1861 MeV/c^2 for $(D^0/\bar{D}^0)$ mass with a standard deviation $\sigma = 21$ MeV/c^2 (χ^2/NDF = 5.5/6) and the signal to noise ratio of $(51 \pm 17)/(38 \pm 13)$. The detection efficiency of $(D^0/\bar{D}^0)$ particles with efficiency of visual inspection taken into account is equal to $\varepsilon(D^0/\bar{D}^0) = 0.036$.

4.2 $D^+ \to K^-\pi^+\pi^+$, $D^- \to K^+\pi^-\pi^-$ decays

For charged mesons we analyzed the $(K\pi\pi)$ systems: $D^+ \to K^-\pi^+\pi^+$, $D^- \to K^+\pi^-\pi^-$. The charged charmed mesons were found by analyzing the events with a three-prong secondary vertex. The selection procedure of events went as follows (more details in [12]):

(i) Search for the third track to be associated with a two-prong secondary vertex taking into account charges and kinematical correspondence to interaction vertex.

(ii) Selection of the $K\pi\pi$ systems with momentum P>7 GeV/c.

(iii) Cutting out non-physical regions and those with the highest background using Dalitz plot for $M(K\pi_1)$ and $M(K\pi_2)$ variables.

(iv) Within three tracks systems, two possible hypotheses for K^0 have shown a significant peak in the mass distribution. Most of background was cut out after applying the condition $M(\pi^+\pi^-)_1$ + $M(\pi^+\pi^-)_2 < 1.2 \text{MeV/c}^2$.

(v) Hypotheses for $(K^-K^+\pi)$ system (possible D_S) were discarded with the $M(K^-K^+\pi) > 1.93$ MeV/c^2 cut.

(vi) Simulations have shown concentration of background events at the smallest decay lengths, the condition $L > 0.12$ mm was applied to eliminate it ($L = L_{vis}$*M/P).

The mass distributions for D^+ and D^- that was obtained with primary selection (i, ii) are shown in Fig. 4. Thay have significant background contributions, eliminated with the rest of cuts (see Fig. 5).
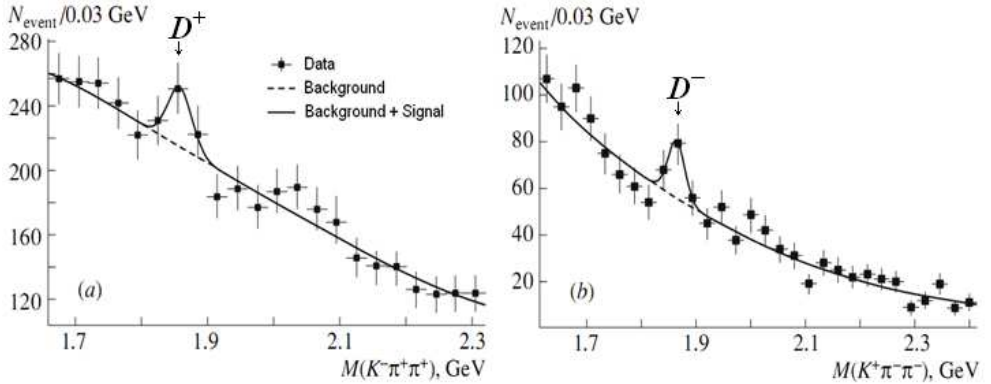
Figure 4. Effective mass spectra of the $K^-\pi^+\pi^+$ (a) and $K^+\pi^-\pi^-$ (b) systems after applying the conditions (i, ii). Data fitted with the sum of a Gaussian function and a sixth order polynomial.

After parameterizing the spectrum in Fig. 5 (left) in terms of the sum of the Gaussian function and a fifth order polynomial (χ^2/NDF = 13.5/30), we got 15.5 ± 5.6 signal events from the D^+ meson decay over the background of 16.6 ± 6.0 events. The measured D^+-meson mass is 1874 ± 5 MeV/c^2 (the world-average value is 1869.6 MeV/c^2) with a standard deviation of 11.5 MeV/c^2. The detection efficiency $\varepsilon(D^+) = 0.014$ was defined from simulations. The same procedure has been applied to search for the D^- meson signal (Fig. 5 right) in the mass spectrum of the $K^+\pi^-\pi^-$. The spectrum was parameterized as a sum of the Gaussian function and the second order polynomial (χ^2/NDF = 3.6/20). The number of events in the signal was 15.0 ± 4.7 over the background of 8.7 ± 2.7 events. The D^--meson mass was 1864 ± 8 MeV/c^2, with the standard deviation of 22 MeV/c^2. The detection efficiency obtained through the simulation for the D^- meson signal was equal to $\varepsilon(D^-) = 0.008$.
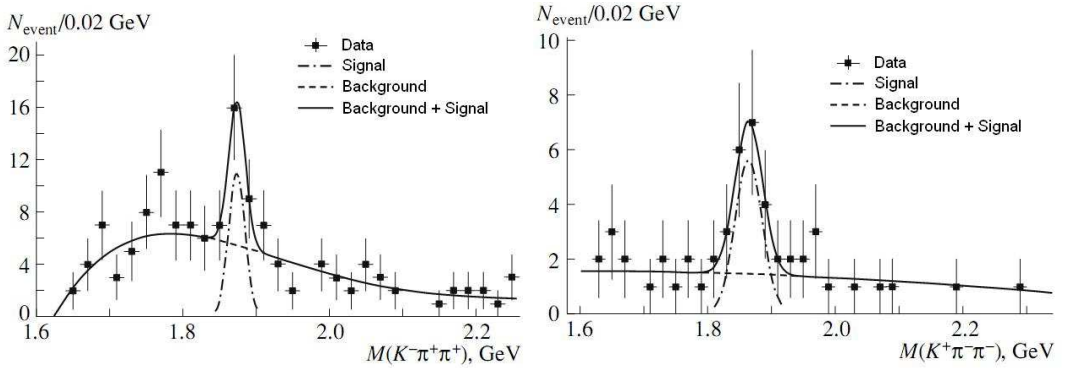
Figure 5. Effective mass spectra of the $K^-\pi^+\pi^+$ (left) and $K^+\pi^-\pi^-$ (right) systems after using all selection criteria.

4.3 $\Lambda_c^+ \to pK^-\pi^+$ **decays**

The charmed Λ_c^+ baryon was analyzed with the three-prong decay $\Lambda_c^+ \to pK^-\pi^+$. The primary procedures were similar to those for the $D^\pm$ mesons decays (i, ii). Without of particle identification, we had two hypotheses for positively charged particles of the $(pK^-\pi^+)$ system in the effective mass spectrum (Fig. 6 left). The next selection procedure of the events was carried out as follows (more details in [13]):

(iii) Dalitz plot for MC events with $M(K^-\pi^+)$ and $M(K^-p)$ variables were used in order to cut out the experimental data background.

(iv) To eliminate the K^0 background, it was required to have for the three-particle system $M(3\pi)$ > 1.2 GeV/c^2. According to simulations, it cuts out about 85% of the background and only 12% of the signal.

(v) The $pK^-\pi^+$ system momentum met the following requirement: $25 < P < 60$ GeV/c.
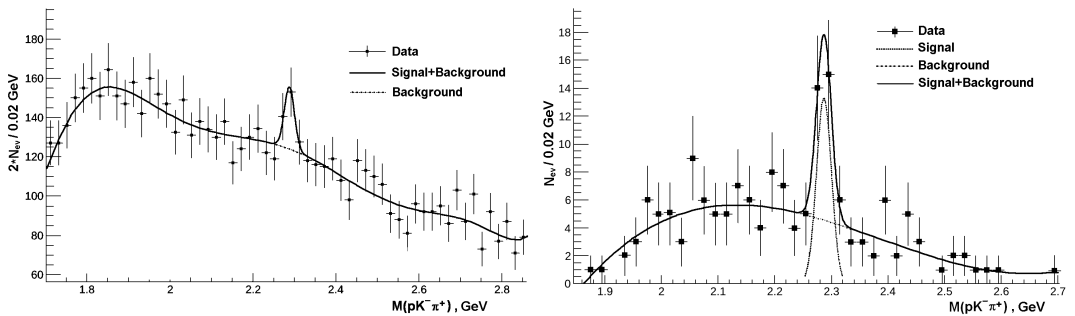
Figure 6. Effective mass spectra of the $pK^-\pi^+$ system (two hypotheses) after the primary selection of events (left) and after using all selection criteria (right).

The application of all the criteria resulted in the effective mass spectrum is shown in Fig. 6 right, with Λ_c^+ signal of 21.6 ± 6.0 events over the background of 16 ± 4 events, the mass 2287 ± 4 MeV/c^2 and $\sigma = 13.1$ MeV/c^2. In case when both of hypotheses turned out to be in the peak region, they are

Table 1. The results of effective mass spectra fitting.

Particle decay	Signal events	Background events	χ^2/NDF	Detection efficiency	Mass, GeV/c^2 (*PDGmass*)
$D^0 \to K\pi$	51±17	38±13	5.5/6	0.036	1861±7 (*1864.8*)
$D^+ \to K^-\pi^+\pi^+$	15.5±5.6	16.6±6.0	13.5/30	0.014	1874±5 (*1869.6*)
$D^- \to K^+\pi^-\pi^-$	15.0±4.7	8.7±2.7	3.6/20	0.008	1864±8 (*1869.6*)
$\Lambda_c^+ \to pK^-\pi^+$	21.6±6.0	16±4	12.7/33	0.011	2287±4 (*2286.5*)

taken with weights of 0.5 (there were 5% of such events in simulations and no one in the experimental data). The effective mass spectrum of the $pK^-\pi^+$ system has been parameterized by the sum of the Gaussian function and the polynomial of the third degree (χ^2/NDF = 12.7/33). The detection efficiency for $\Lambda_c^+ \to pK^-\pi^+$ was equal $\varepsilon = 0.011$. The summary results of fitting the effective mass charmed particles spectra are presented in Table 1.

5 Cross sections for charmed particle production and their A-dependence

The following relation has been used to calculate the inclusive cross sections for a given charmed particle:

$$N_s(i) = [N_0 \times (\sigma(i) \times A^\alpha)/(\sigma_{pp} \times A^{0.7})] \times [(B(i) \times \varepsilon(i))/K_{tr}],$$

where $i = D^0, \bar{D}^0, D^+, D^-$ or Λ_c^+; $N_s(i)$ is the number of events in the signal for (i) type of the charmed particle produced in the given target; N_0 is the number of inelastic interactions in this target; $\sigma(i)$ is the cross section for charmed particle (i) production at a single nucleon of the target; A is the atomic mass number of AT material (C, Si or Pb); $\alpha(i)$ is an exponent parameter in A-dependence of the charm cross section; σ_{pp} is the cross section of the inelastic proton-proton interaction at 70 GeV (= 31440 μb); $B(i)$ is the branching ratio for the charmed particle decay ($B(D^0/\bar{D}^0) \to K\pi$) = 0.038, $B(D^\pm \to K\pi\pi)$ = 0.094, $B(\Lambda_c^+ \to pK^-\pi^+)$ = 0.05); $\varepsilon(i)$ is the detection efficiency of the charmed particle from Table 1 and $K_{tr} = 0.57$ is the trigger efficiency of registration of inelastic events in our experiment.

Substituting $C(i) = [N_0/(\sigma_{pp} \times A^{0.7})] \times [B(i) \times \varepsilon(i)/K_{tr}]$, the relation takes the following form: $N_s(i) = C(i) \times \sigma(i) \times A^\alpha$ or $\ln(N_s(i)) = \alpha \times \ln(A) + \ln(\sigma(i))$. Figure 7 shows A-dependences of the charmed particles production in AT.

The parameter α obtained from the straight linear approximations in Fig. 7 for each particle is presented in Table 2 together with inclusive cross section and path length. The α-parameters are close to 1 for all charmed particles, as it was found earlier for the hidden charm (J/ψ and ψ') production cross sections in the proton-nucleus interactions [14], [15], [16], [17].

On the basis of results presented in Table 2 and using the relation [18]

$$\sigma_{tot}(c\bar{c}) = 0.5 \cdot (\sigma_{D+} + \sigma_{D0} + \sigma_{D-} + \sigma_{\bar{D}0} + \sigma_{\Lambda c+} + \sigma_{Ds} + \sigma_{\bar{D}s})$$

total cross section of the charmed particles production in proton-nucleon interactions at 70 GeV can be estimated as $\sigma(c\bar{c}) = 7.1 \pm 2.3(stat) \pm 1.4(syst)$ μb/nucleon. The charmed particles yields measured in our experiment are given in Table 3 and in Fig. 8 along with the data from other experiments and theoretical predictions.

The contributions of charmed particles to the total cross section vary with energy. For example, the particles (D^0 and D^+) contributions go down as the interaction energy decreases to 70 GeV, while
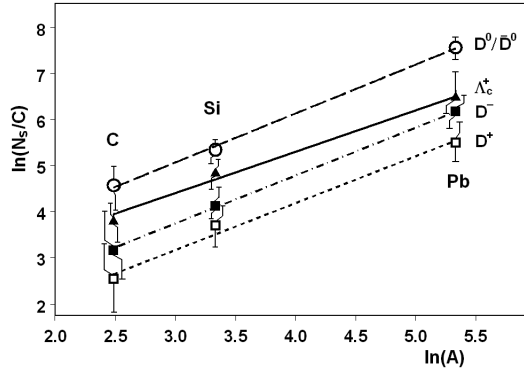
**Figure 7.** The A-dependence of cross sections for the charmed particles production in pA-interactions.

Table 2. Characteristics of the charmed particles production. The first error is statistical, the second – the systematical one.

Num	Type of charmed particle	Inclusive cross section for all x_F (μb/nucleon)	α-parameter	$c\tau$, mm	
				SVD-2	PDG
1	D^+	1.2±0.4±0.2	1.02±0.26	0.291±0.075	0.311
2	D^-	1.9±0.6±0.4	1.04±0.27	0.341±0.088	0.311
3	D^0	2.5±0.8±0.5	1.08±0.12	0.123±0.024	0.124
4	$\bar{D}^0$	4.6±1.6±0.9			
5	$D^0/\bar{D}^0$	7.1±1.8±0.9			
6	Λ_c^+	4.0±1.6±1.2	0.9±0.2	0.051±0.011	0.059

Table 3. The charmed particles yields, $\sigma(i)/\sigma_{tot}(c\bar{c})$.

Yields \ particle	PYTHIA pp	FRITIOF pA	SVD-2 pA	Other experiments	
				NA-27 [23]	HERA-B [24]
D^0	0.28	0.51	0.35±0.16	0.57±0.08	0.44±0.18
$\bar{D}^0$	0.74	0.59	0.65±0.31	0.43±0.09	0.54±0.23
D^+	0.13	0.29	0.16±0.07	0.31±0.06	0.19±0.08
D^-	0.24	0.27	0.27±0.17	0.34±0.06	0.25±0.11
Λ_c^+	0.55	0.36	0.56±0.27	0.52±0.35 | 0.42±0.13 | 0.18±0.01 BIS-2 [25] | E-769 [26] | SELEX-2 [27]	

the antiparticles ($\bar{D}^0$, D^- and Λ_c^+) contributions grow. A large difference of the charmed particle and antiparticle yields was firstly observed experimentally in neutron–nucleus interactions at the average neutron-beam energy of 43 GeV in the BIS-2 experiment [19]. Only antiparticle ($\bar{D}^0$ and D^-) decays were observed there, while particle (D^0 and D^+) decays were not found (their cross sections proved to be below the sensitivity threshold). The results shown in Fig. 8 are compatible with the predictions of the statistical hadronization model [18], [20].
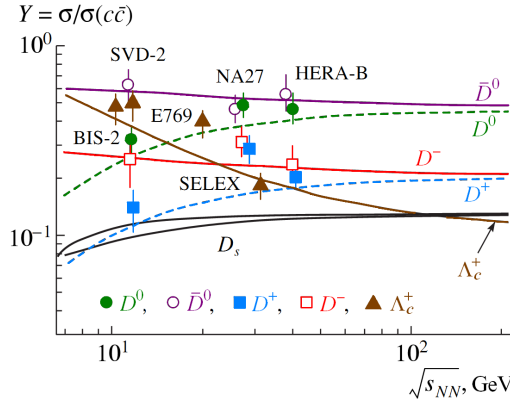
Figure 8. Relative yields of charmed particles. The experimental points are taken from Table 3, the theoretical curves (with designation of a particle) are taken from [18].

6 Results

We present total cross section for open charm production and cross sections for the inclusive production of D mesons and Λ_c^+ baryon.

- The total open charm production cross-section at the collision c.m. energy $\sqrt{s} = 11.8$ GeV is well above QCD models predictions and inclusive cross sections are close to the prediction of QGSM for D mesons and for Λ_c^+ baryon at this energy (Fig. 9 left).
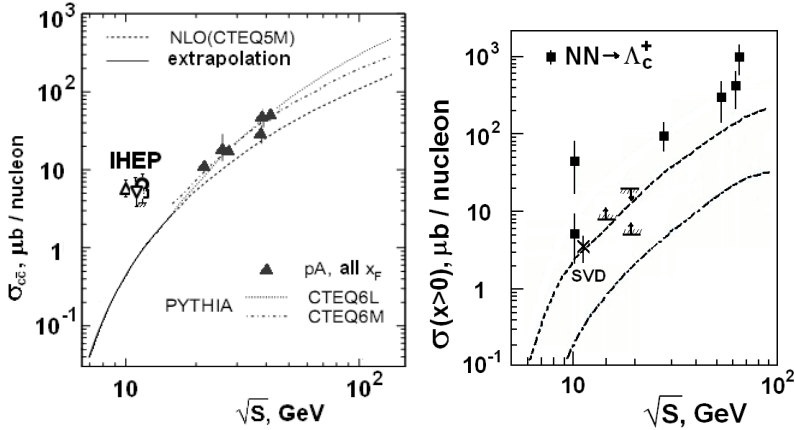
Figure 9. Left: The total cross section for charm production in pA-interactions from [1] - [3], [18]. Extrapolation (solid line) was carried out without points from IHEP: ◯ - SVD-2 experiment (see above), ▽ - beam-dump experiment with muon absorber [1], ⊔ - SCAT bubble chamber experiment [2] and △ -the experiment with BIS-2 spectrometer [3]. Other lines are from various models [18]. Right: The inclusive cross section for Λ_c^+ baryon production at $x_F > 0$. The experimental data are from [25], [28] - [29] (CERN, FNAL, BIS-2), point (X) is from our experiment. Dashed lines are for predictions of two versions of QCD model [25].

- The cross sections for Λ_c^+ production (Fig. 9 right) at the collision c.m. energy $\sqrt{s} > 30$ GeV contradict the total cross sections for the open charm production (Fig. 9 left). The experimental cross sections for Λ_c^+ are extraordinarily large in this area.

- The contributions of inclusive charmed particle cross-sections into the total one vary at lower collision energies.

7 Acknowledgements

References

[1] A.E. Astratyan et al, Phys. Lett. B **79**, 497 (1978).

[2] V.V. Ammosov et al, Physics of Atomic Nuclei, **53**, 999 (1991).

[3] A.N. Aleev et al, Physics of Atomic Nuclei, **56**, 147 (1993).

[4] V.V. Avdeichikov et al, Instruments and Experimental Techniques, **56**, 9 (2013).

[5] H.Pi, Computer Physic Communication, **71**, 173 (1992).

[6] G. Alexander et al. OPAL collaboration, Zeit. fur Physik C **72**, 16 (1996).

[7] G.S. Huang et al, Phys. Rev. Letters, **94**, 011802 (2005)

[8] GEANT 3.21, CERN Program Library Long Write Up W5013.

[9] A.A. Kiriakov et al, Instruments and Experimental Techniques, **47**, 611 (2004).

[10] A.P. Vorobiev et al, IHEP Preprint 2008-17, Protvino, 2008 (in russian). http://web.ihep.su/library/pubs/prep2008/ps/2008-17.pdf

[11] V.N. Ryadovikov (on behalf of the SVD-2 Collab.), Physics of Atomic Nuclei, **73**, 1539 (2010).

[12] V.N. Ryadovikov (on behalf of the SVD-2 Collab.), Physics of Atomic Nuclei, **77**, 716 (2014).

[13] V.N. Ryadovikov (on behalf of the SVD-2 Collab.), Physics of Atomic Nuclei, **79**, 144 (2016).

[14] J. Badier et al, Z.Phys. C - Particle and Fields **20**, 101 (1983).

[15] D.M. Alde et al, Phys. Rev. Letters, **66**, 133 (1991).

[16] M.C. Abreu et al, Physics Letters, B **410**, 327 (1997).

[17] M.J. Leitch et al, Nuclear Physics, A **544**, 197 (1992).

[18] A. Andronic, P. Braun-Munzinger, K. Redlich, J. Stachel, Phys. Lett. B **659**, 149 (2008). arXiv:0708.1488

[19] A. Aleev et al, Z.Phys. C - Particle and Fields **37**, 243 (1988).

[20] A. Andronic, F. Beutler, P. Braun-Munzinger et al., arXiv:0904.1368v2

[21] R.Vogt, Phys. Rev. C **61**, 035203 (2000).

[22] A.N. Aleev et al, SVD-2 Collaboration, Physics of Atomic Nuclei, **74**, 324 (2011).

[23] M. Aguilar - Benitez, Na-27 Collaboration, Phys. Letters, B **189**, 476 (1987).

[24] I. Abt et al, Eur. Phys. J. C **52**, 531 2007. http://arxiv.org/abs/0708.1443v1

[25] A. N. Aleev et al., BIS-2 Collaboration, Z.Phys. C - Particle and Fields, **23**, 333 (1984). E. N. Chudakov, Master's Thesis (1987), JINR Preprint 1-87-183, 1987 (in russian)

[26] J. Engelfried, www.ifisica.uaslp.mx/ jurgen/public/dpc99-talk.ps.gz, 1999.

[27] F.G. Garcia et al., SELEX Collaboration, Phys. Lett. B **528**, 49 (2002). http://arxiv.org/pdf/hep-ex/0109017.pdf

[28] Bailay R. et al., Nucl. Phys. B **239**, 15 (1984).

[29] M. Basile et al., Lett. Nuovo Cimento, **30**, 487 (1981). M. Basile et al., Lett. Nuovo Cimento, **30**, 481 (1981). F. Muller, Proceedings of IV Warsaw Symposium, 1981 G. Bari et al., Nuovo Cimento, A **104**, 571 (1991).